Fractal Diffusion in Smooth Dynamical Systems with Virtual Invariant Curves[¶]

B. V. Chirikov* and V. V. Vecheslavov**

Budker Institute of Nuclear Physics, Novosibirsk, 630090 Russia
*e-mail: chirikov@inp.nsk.su
**e-mail: vecheslavov@inp.nsk.su
Received April 5, 2002

Abstract—Preliminary results of extensive numerical experiments with a family of simple models specified by the smooth canonical strongly chaotic 2D map with global virtual invariant curves are presented. We focus on the statistics of the diffusion rate D of individual trajectories for various fixed values of the model perturbation parameters K and d. Our previous conjecture on the fractal statistics determined by the critical structure of both the phase space and the motion is confirmed and studied in some detail. In particular, we find additional characteristics of what we earlier termed the virtual invariant curve diffusion suppression, which is related to a new very specific type of critical structure. A surprising example of ergodic motion with a "hidden" critical structure strongly affecting the diffusion rate was also encountered. At a weak perturbation ($K \ll 1$), we discovered a very peculiar diffusion regime with the diffusion rate $D = K^2/3$ as in the opposite limit of a strong ($K \gg 1$) uncorrelated perturbation, but in contrast to the latter, the new regime involves strong correlations and exists for a very short time only. We have no definite explanation of such a controversial behavior. © 2002 MAIK "Nauka/Interperiodica".

1. INTRODUCTION: VIRTUAL INVARIANT CURVES

In a two-dimensional map (2.1) that we study here, the diffusion crucially depends on the global invariant curves (GICs) that cut the 2D phase space of the motion (a cylinder, see the next section). Even a single such curve is sufficient to completely block the global diffusion in the action variable along the cylinder. As is well known by now, the existence of GICs depends not only on the perturbation strength but also on its smoothness. It is convenient to characterize the latter by the temporal Fourier spectrum of the perturbation. For an analytical perturbation, the Fourier amplitudes decay exponentially fast. In this case, the global diffusion sets up if the perturbation $\epsilon \gtrsim \epsilon_{cr}$ exceeds some critical value. Otherwise, the chaos remains localized within relatively narrow chaotic layers of nonlinear resonances. As a result, either the global diffusion is completely blocked by GICs or the rate of the diffusion and the measure of its domain decay exponentially in the parameter $1/\epsilon$ as $\epsilon \longrightarrow 0$ (the so-called Arnold diffusion; see, e.g., [1–3] for a general review).

By definition, the Hamiltonian of a smooth system has the power-law Fourier spectrum with a certain exponent $\beta + 1$ (see, e.g., [4] and references therein). In this case, the global diffusion is always blocked for some sufficiently small perturbation strength $\epsilon < \epsilon_{cr}(\beta)$ if the smoothness parameter $\beta > \beta_{cr}$ exceeds the critical value. This is similar to the case of an analytical Hamil-

tonian except that the critical perturbation now depends on the Hamiltonian smoothness ($\epsilon_{cr}(\beta) \longrightarrow 0$ as $\beta \longrightarrow \beta_{cr}$).

To the best of our knowledge, the strongest rigorous result is that $\beta_{cr} < 4$ for a 2D map as in this paper (see [5]). But a simple physical consideration [4] leads to an even smaller value $\beta_{cr} = 3$, which is still to be confirmed somehow, theoretically or numerically. In any event, the smoothness $\beta = 2$ of our model here is even less.

Until recently, the behavior of dynamical systems in the opposite case $\beta < \beta_{cr}$ of a poor smoothness remained rather vague. Even though most of the numerical data seemed to confirm the simplest behavior of some universal global diffusion (see, e.g., [6]), several counterexamples were also observed (see, e.g., [7, 8]).

In these counterexamples, some trajectories remained within a certain restricted part of the phase space for a sufficiently long computation time. No clear explanation of these strange events has yet been given.

Meanwhile, about 20 years ago (!) a number of mathematical studies revealed various possibilities for the existence of GICs in smooth systems with $\beta < \beta_{cr}$ (see, e.g., [8–10]). To us, the most comprehensive analysis of this problem was given by Bullett [9], who rigorously proved a strange survival of infinitely many GICs amid a strong local chaos. Surprisingly, all these interesting results remain essentially unknown, at least to physicists. Apparently, this is because the above mathematical papers were restricted (perforce!) to what could be done rigorously, that is, to the invariant curves

---

[¶]This article was submitted by the authors in English.

only, without any attempt to analyze very interesting and important transport processes such as diffusion. This is still within reach of physical analysis and numerical (or laboratory) experiments only. As a result, only after the recent accidental rediscovery of GICs in chaos by Ovsyannikov [11] (which is still unpublished; see [12, 13] for the full text of Ovsyannikov's theorem) have intense physical studies of this interesting phenomenon begun [12–16].

Interestingly, the authors of both [9] and [11] used exactly the same model, in which a strange locked-in trajectory was observed much earlier [7]. Apparently, this is because this model (a particular case of our model with the parameter $d = 1/2$; see Section 2) is the simplest one possessing those curious GICs (see [15] for discussion). Perhaps the main surprise was that the GICs include the separatrices of nonlinear resonances, which have always been considered as ones destroyed first by almost any perturbation. The principal difference is that the invariant curves, separatrices including, now exist for special values of the system parameters only (e.g., $K = K_m$).

Although there are infinitely many such special values of the parameter and infinitely many GICs such that a single GIG completely blocks the global diffusion for each of the parameter values, the probability of global diffusion (that is, the measure of such K values) is apparently zero. Therefore, a principal question to be answered is: What would be the behavior of that system for an arbitrary value of K? In [16], we conjectured that, even though the set of K_m is not everywhere dense [9] in general, the density of this set is rather high, and we can therefore expect some change (presumably suppression) of the diffusion for every K value compared to the "usual" (familiar) dynamical system. In other words, we hypothesized that the structure of the phase space and of the motion therein can be changed by the formation of GIG at a close K value even if no GICs occur for almost all K. This is why we now call such a neighbor-K invariant curve the virtual one (VIC) with respect to any K [16].

Preliminary numerical experiments presented in [16] did confirm our conjecture. These experiments were done by the prompt computation of the average diffusion rate $D(K)$ as a function of the parameter K in the domain with GICs, real or virtual ones. The experiments revealed a very strong suppression of the diffusion, up to many orders of magnitude, restricted only by the computation time. But even more interestingly, a very complicated (apparently fractal) structure of the dependence $D(K)$ was revealed. This seems to be a result of a very complicated structure of the model phase space itself. Preliminarily, it looks like the so-called critical structure (see, e.g., [4]), but a rather specific one due to a forest of VICs.

In the present paper, we begin the study of this seemingly new type of the critical structure. Specifically, we start with the investigation of the statistical
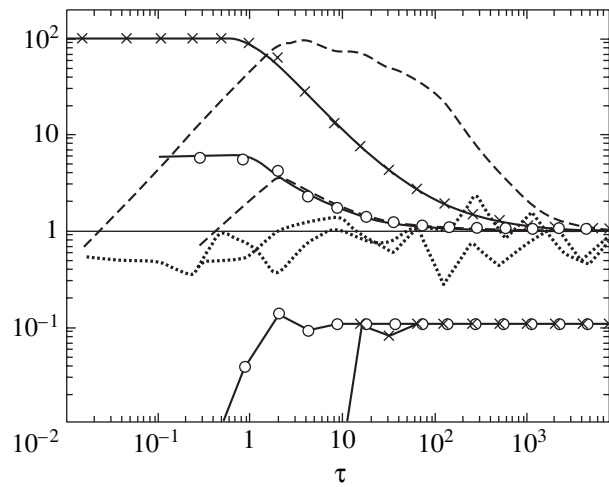

Fig. 1. The diffusion relaxation $D^*(\tau) = D(\tau)/D_\infty \longrightarrow 1$ in model (2.2) with the parameter $d = 0$ (without invariant curves) is presented as a function of the dimensionless time τ [Eq. (3.5)] for the two values $K = 0.01$ (circles) and $K = 3 \times 10^{-5}$ (crosses). Two smooth solid lines show empirical relation (3.5) with two fitting parameters $c = 1$ and $\gamma = 4$. Dashed lines are variances the $V_M(\tau)$ in Eq. (3.2), and dotted lines show the variances $V_N(\tau)$ in Eq. (3.8). In the lower part, the scaling in Eq. (3.6) is presented reduced by the factor 10 to avoid overlapping with other data. The full volume of empirical data is $J = M \times N = 10^4 \times 10 = 10^5$.

properties of diffusion as one of the characteristic processes in chaotic motion.

2. MODEL: THE SAME AGAIN

For the reader's convenience, we here repeat the description of the model in [15, 16]. In the canonical variables given by the action (momentum) p and the phase x, the model is specified by the map

$$\bar{p} = p + Kf(x), \quad \bar{x} = x + \bar{p} \quad \text{mod } 1, \qquad (2.1)$$

where $K = \varepsilon > 0$ is the perturbation strength (not necessarily weak) and the "force" $f(x)$ is the antisymmetric piecewise linear "saw" of period 1 ($f(-y) = -f(y)$, $y = x - 1/2$). The phase space of the model is the cylinder $0 < x < 1$, $-\infty < p < +\infty$.

As in [15, 16], we actually consider a family of maps with another parameter d (see Fig. 1 in [15]) and the force

$$f(x) = \begin{cases} \dfrac{2x}{1-d}, & |x| \leq \dfrac{1-d}{2} \\[2mm] -\dfrac{2y}{d}, & |y| \leq \dfrac{d}{2}, \end{cases} \qquad (2.2)$$

where $y = x - 1/2$ and the second parameter d ($0 \leq d \leq 1$) is the distance between the two "teeth" of the saw $|f(x)| = 1$ at the points $y = y_\pm = \pm d/2$. The most studied particular case of the family corresponds to $d = 1/2$,

where the saw $f(x)$ with two teeth is symmetric. In the limit $d = 0$, the two teeth merge into one and all the invariant curves are destroyed. This was observed and explained in [15] for $K > 0$. In the opposite case, where $K < 0$ (which is equivalent to $K > 0$, $d = 1$), the dynamics of the model is completely different, and we do not consider it in this paper (see [15] for a brief discussion). In our 2D map (2.1), the GIC supports rotation of the phase x around the cylinder, which bars any motion in p over GICs. In contrast to this, a local invariant curve (LIC) surrounding, e.g., the domain of regular motion (see [4] and Section 5 below) corresponds to oscillation in the phase x, which allows other trajectories to bypass that obstacle.

The GICs, separatrices including, exist in the entire interval $0 < d < 1$, but for special K values only [9, 15, 16]. In particular, the invariant curves are completely absent [9] for sufficiently large parameter values

$$K > K_B(d) = \frac{2d^2}{1 + d}, \quad 0 < d < 1. \tag{2.3}$$

If $K \gg K_B$ (see below), the physical quantity of main interest to us, the diffusion rate D, can be approximately calculated from the Fourier expansion of force (2.2) (see [16] for details)

$$f(x) = \sum_{n \geq 1} \frac{f_n}{n^\beta} \sin(2\pi nx), \tag{2.4}$$

where

$$f_n = -\frac{2}{\pi^2} \frac{\cos(n\pi)\sin(n\pi d)}{d(1 - d)}, \quad \beta = 2. \tag{2.5}$$

In particular, in the limit $d = 0$,

$$f_n = -\frac{2}{\pi}\cos(n\pi), \quad \beta = 1, \tag{2.6}$$

the smoothness parameter β becomes less by one but both values are less than the critical one $\beta_{cr} = 3$.

The diffusion rate and other quantities are calculated using the standard analysis of nonlinear resonances and their interaction (overlap) (see, e.g., [1–3, 16]). The calculation is especially simple if we neglect the variation of the coefficients $|f_n| \approx$ const in (2.4). This simplification is exact for $d = 0$ [see (2.6)] and remains reasonably accurate [16] for

$$K \gtrsim 3K_B = \frac{6d^2}{1 + d}. \tag{2.7}$$

The diffusion rate is then approximately given by a very simple standard relation

$$D(K) = \frac{\overline{(\Delta p)_t^2}}{t} \approx \frac{256}{\pi^5}K^{5/2} \approx 0.57 K^{5/2}, \tag{2.8}$$

where t is the motion time in map iterations and the parameter $K \ll 1$ is assumed to be sufficiently small.

The latter expression in (2.8), which we use below, is the result of extensive numerical experiments in [6], also confirmed in [16] for $K \lesssim 0.1$ (see [16] and Section 3).

We note that the dependence $D(K) \propto K^{5/2}$ is different from the usual, or, better to say, the simplest, one $D(K) \propto K^2$. This is explained by the dynamical correlation of motion that is determined by the frequency of the phase oscillation on nonlinear resonances,

$$\Omega_n = \sqrt{\frac{2\pi K f_n}{n^{\beta-1}}} \approx 2\sqrt{K} \approx \Lambda_n(K) \ll 1, \tag{2.9}$$

where Λ_n stands for the Lyapunov exponent charaterizing the local exponential instability of the motion, which is the main criterion for dynamical chaos. We note that for $\beta = 1$, both Ω_n and Λ_n are independent of the Fourier harmonic number n. The exact value of the Lyapunov exponent in the limit $d = 0$ is given by

$$\Lambda = \ln(1 + K + \sqrt{2K + K^2}) \approx \sqrt{2K} \ll 1. \tag{2.10}$$

The latter expression is the approximation for small K [cf. Eq. (2.9)], which is sufficiently good within the region of Eq. (2.8) ($K \lesssim 0.1$) with the accuracy of ~1%. Because the time is discrete in our model (the number of the map iterations), both correlation characteristics, Eqs. (2.9) and (2.10), must be small, which implies the above restriction on the parameter K.

In the opposite limit $K \gg 1$, the correlation between successive x values is negligible, and we arrive at the "usual" relation for the diffusion rate,

$$D(K) = K^2 \int_0^1 f^2(x)dx = \frac{K^2}{3}, \tag{2.11}$$

which is independent of the parameter d. In the intermediate region ($K \sim 1$), the correlation causes a decaying oscillation (see [6]), which is beyond the scope of the present paper.

3. DIFFUSION WITHOUT ANY INVARIANT CURVES: AVERAGES AND MOMENTS

As mentioned above, there are no invariant curves for $d = 0$. Moreover, the motion is ergodic, which implies the simplest structure of the phase space (cf. Section 4 below). Therefore, this particular case is not of the main interest to us by itself. It is nevertheless a good introduction to our central problem considered in Section 6 below. A similar approach was taken in our previous paper [16].

We first consider the time dependence of the diffusion rate $D(K; t)$. The semicolon instead of the usual comma is intended to emphasize that this time dependence is not a real physical contribution to the diffusion but rather a combination of two different processes: the proper diffusion via accumulation of random perturba-

tion effects and a stationary regular oscillation of the diffusing variable (p in our case), which is a certain type of background for the diffusion. This phenomenon can be roughly represented by the simple relation

$$D(K; t) \sim D_\infty(K) + \frac{B(K)}{t}, \qquad (3.1)$$

where $B(K)$ is some function of the perturbation (see, e.g., [16] and Eq. (3.5) below). In other words, in many cases, the present studies including, the nondiffusing stationary part can be separated from the diffusing part, thereby considerably simplifying the analysis of this complicated process. All this can be described, of course, via the standard method of the correlation of perturbation. But this would lead to much more intricate theoretical relations and, in addition, to much less information on the diffusion dynamics (see, e.g., [6]).

An example of the diffusion kinetics is presented in Fig. 1. The computation was done as follows. The number of trajectories $M \gg 1$ with random initial conditions homogeneously distributed within the unit area of the phase cylinder ($0 \le x_0 < 1$, $0 \le p_0 < 1$) were run for a sufficiently long time with successive outputs at certain intermediate moments of time t as shown in Fig. 1. We recall that t is measured in the number of the map iterations. Each output includes the diffusion rate (D), averaged over all M trajectories and the dimensionless variance

$$V_M = \frac{\langle D^2 \rangle - \langle D \rangle^2}{2 \langle D \rangle^2}. \qquad (3.2)$$

For the Gaussian distribution of the action p, this variance must be equal to unity. This is indeed the case for a sufficiently long motion time when the measured diffusion rate reaches its asymptotic value D_∞ in Eq. (3.1). A quite different dependence $V_M(t)$ for the previous smaller time is not surprising (nor is it very interesting) because $D(t)$ then depends on a completely different physical process that must be passed over.

A real surprise was the very beginning of the diffusion, the plateau in Fig. 1. This looks like a real diffusion unlike the following part of the stationary oscillation. Moreover, the diffusion rate $D_0 = K^2/3$ on the plateau is the maximum one, Eq. (2.11), as for $K \gg 1$. Another interesting observation is the duration of this strange diffusion,

$$t_0 \approx \frac{1}{\Lambda} \approx \frac{1}{\sqrt{2K}}, \qquad (3.3)$$

which is close to the inverse Lyapunov exponent, the rise time of the local exponential instability of the underlying chaotic motion. The last but not the least curious property is the fast increase in variance (3.2),

$$V_M(t) \approx \frac{t}{3}, \quad 2 \le t \lesssim t_0, \qquad (3.4)$$

as shown in Fig. 1. This is qualitatively different from the behavior of the same diffusion rate for $K \gg 1$ with the usual variance $V_M \approx 1$. The dynamical mechanism of this strange transitional diffusion is not completely clear and requires further studies. Apparently, it is somehow related to the main correlation (2.9) on dynamical scale (3.3). Although the initial "diffusion" is relatively fast, it lasts for only a short time, and the relative change of the initial distribution of trajectories

$$\frac{|\Delta p|}{|\Delta p|_0} \sim \sqrt{\frac{D_0}{\Lambda}} \sim K^{3/4} \ll 1$$

is therefore negligible for $K \ll 1$ unless the initial distribution $|\Delta p|_0 \lesssim K^{3/4}$ is very narrow. But in the latter case, the dependence $D(t)$ is very sensitive to the form of the initial distribution in p, as several of our preliminary numerical experiments reveal. The variance of $D(t)$ is especially strong for small $t \sim t_0$ in the region of that mysterious plateau but eventually decays as $t \longrightarrow \infty$, with the diffusion approaching its limit value D_∞. Apparently, this is related to a complicated fine structure of the phase space and/or of the motion correlations. This interesting question certainly deserves further studies, but in the present paper, we consider the simplest, homogeneous, distribution of the trajectory initial conditions on the phase cylinder.

In this particular case, a very simple and surprisingly accurate empirical relation for the diffusion time dependence has been found starting from the qualitative picture in (3.1). It is given by

$$D(t) \approx \frac{D_0 + \tau D_\infty}{(1 + \tau^\gamma)^{1/\gamma}}, \quad \tau = c\Lambda t, \qquad (3.5)$$

where τ is the dimensionless time with an empirical fitting parameter c that is very close to one. The second empirical parameter $\gamma \approx 4$ is less definite, but it affects the turn of the dependence $D(t)$ at $\tau \approx 1$ only. This relaxation of the diffusion rate has two time scales: the plateau

$$\tau_{\text{pl}} = 1 \text{ or } t_{\text{pl}} = 1/c\Lambda \approx 1/\sqrt{2K} \gg 1$$

and the relaxation

$$\tau_R = D_0/D_\infty \sim 1/\sqrt{K} \gg 1 \text{ or } t_R \sim 1/K,$$

which is much longer. Interestingly, the usual diffusion spreading of a very narrow initial p distribution on the relaxation time scale

$$|\Delta p|_R^2 = D_\infty t_R = \frac{D_\infty(D_0/D_\infty)}{c\Lambda} = \frac{D_0}{c\Lambda} = |\Delta p|_{\text{pl}}^2$$

is exactly equal to the spreading on the plateau. Hence, the full relaxation spreading is twice as large, which is also directly seen from empirical relation (3.5),

$$|\Delta p|_R^2 = D(\tau_R)\frac{\tau_R}{c\Lambda} \approx \frac{D_0 + \tau_R D_\infty}{(1 + \tau_R^\gamma)^{1/\gamma}}\frac{\tau_R}{c\Lambda} \sim K^{3/2} \ll 1,$$

and which is still much less than the unit p period.

In Fig. 1, empirical relation (3.5) is presented and compared with the numerical data in the dimensionless variables τ and $D^* = D/D_\infty$, where D_∞ is the asymptotic ("true") diffusion rate (2.8). In these variables, the curves with various K values are similar and converge in the limit as $\tau \longrightarrow \infty$.

Another interesting scaling can be done as follows. We calculate the diffusion rate $D_\infty(D(\tau)) = D_{th}$ from Eq. (3.5) and plot its ratio to the true rate in Eq. (2.8),

$$\frac{D_{th}}{D_\infty} \approx \frac{D(\tau)(1 + \tau^\gamma)^{1/\gamma} - D_0}{\tau D_\infty} \approx 1. \qquad (3.6)$$

Then, within the accuracy of scaling (3.5) and of fluctuations, this ratio must always be close to unity. This is indeed the case except on the plateau ($t \lesssim t_0$), where the rate $D(\tau)$ is almost independent of τ (see Fig. 1). The next important statistical property consists in fluctuations of the diffusion rate. One characteristic of these fluctuations is the dispersion of trajectories, which is characterized by the variance in Eq. (3.2). If all the trajectories were statistically independent, the dispersion of the mean diffusion rate would be

$$\left(\frac{\Delta\langle D\rangle}{\langle D\rangle}\right)^2 = \frac{2V_M}{M-1}. \qquad (3.7)$$

By construction, the trajectories are indeed independent with respect to their initial conditions but not necessarily with respect to the corresponding diffusion rate. To verify this, we repeated the computation of the diffusion N times with new and independent initial conditions and then calculated the second (new) dimensionless variance for the average diffusion rate,

$$V_N = \left(\frac{\langle\langle D\rangle^2\rangle_N}{\langle\langle D\rangle\rangle_N^2} - 1\right)\frac{M-1}{2V_M} \approx 1. \qquad (3.8)$$

Again, if Eq. (3.7) is valid, the variance V_N must be close to one.

The time dependence of both variances, $V_M(t)$ and $V_N(t)$, is shown in Fig. 1. Remarkably, their behavior is qualitatively different. The first variance $V_M(t)$ depends on the distribution function of p in the ensemble of trajectories, while the second variance $V_N(t)$ is affected by the statistical dependence (or independence) among trajectories for any distribution function. The results of our numerical experiments presented in Fig. 1 clearly demonstrate that the distribution in p quickly deviates from the Gaussian one during the diffusion on the plateau and returns only in the limit as $t \longrightarrow \infty$, when the diffusion rate $D \longrightarrow D_\infty$ approaches the asymptotic value without any nondiffusing part. Unlike this, the trajectories remain statistically independent during the

entire process of the diffusion relaxation. We return to this interesting point in Section 7.

We now consider the most informative statistical characteristic, the distribution function $f(D)$ of the diffusion rate.

4. DIFFUSION WITHOUT INVARIANT CURVES: THE DISTRIBUTION FUNCTION

In the main part of our paper (Section 6), we are primarily interested in the distribution tail $D \longrightarrow 0$ of a very low diffusion rate. The shape of this tail is known to be an important characteristic of the critical structure of the motion (see, e.g., [4]). The first indications of such a structure in the presence of virtual invariant curves were observed in [16]. Here, we continue these studies.

Because the statistics of the far tail are always rather poor, we follow [16] in using a special version of the integral distribution

$$F(D) = \int_0^D f(D')dD' \approx \frac{j}{J}, \qquad (4.1)$$

the so-called "rank-ordering statistics of extreme events" (see, e.g., [17]). The following simple ordering of the $D(j)$ values (events) of the diffusion rate is sufficient for this: $D(j+1) > D(j), j = 1, 2, \ldots, J$. The integral probability is then approximately given by the ratio j/J, as shown in Eq. (4.1).

In computation, we typically ran M trajectories N times (see Section 3), and the maximum number of events therefore reached $J = M \times N = 10^4 \times 10 = 10^5$. To obtain the lowest possible D values and simultaneously minimize a rather big output, we ordered all the computed events but printed only J_0 of those, with $J_0 \ll J$, such that some (the smallest) D_j were obtained first, while the rest were printed on a logarithmic scale. An example of such a distribution is presented in Fig. 2 for $K = 0.001$ in the variables $D^* = D/\langle D\rangle$ and $F(D^*) = j/J$, where $\langle D\rangle$ is some average diffusion rate (see below). The upper distribution corresponds to a rather long motion time $t = 10^4 \gg 1/K$, with the mean diffusion rate already very close to the limit D_∞. For the lower distribution, $t = 10$ is very short and corresponds to the plateau.

At least in the former case, where the p distribution is Gaussian (see Section 3), the distribution

$$f(D) = \frac{\alpha^\lambda}{\Gamma(\lambda)}D^{\lambda-1}e^{-\alpha D} \qquad (4.2)$$

is the so-called Pearson Γ distribution with the two moments

$$\langle D\rangle = \frac{\lambda}{\alpha}, \quad (\Delta D)^2 = \langle D^2\rangle - \langle D\rangle^2 = \frac{\lambda}{\alpha^2}, \qquad (4.3)$$
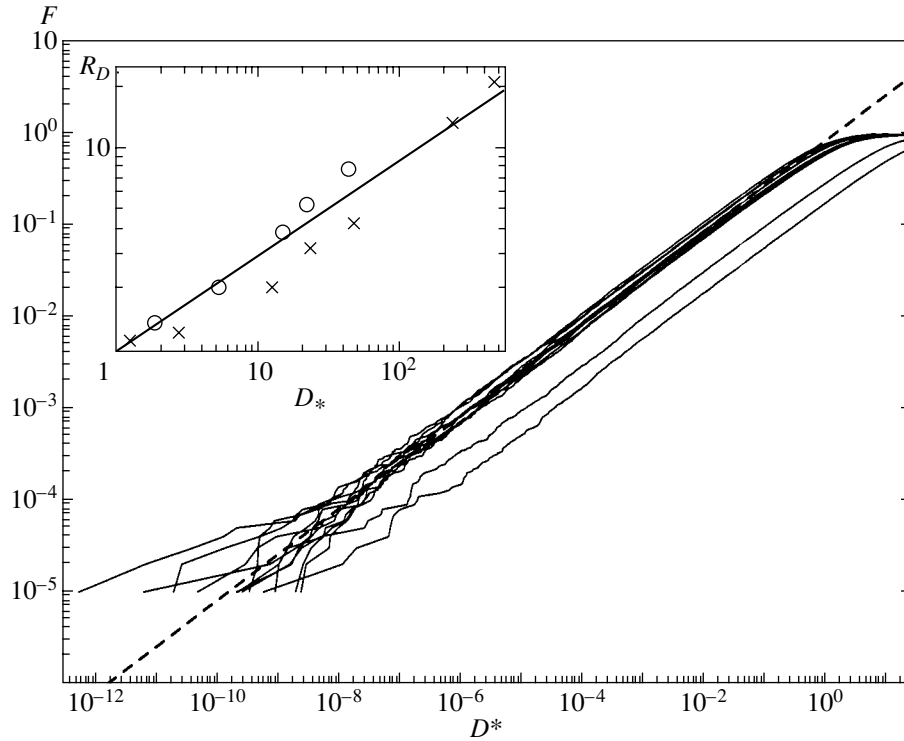
Fig. 2. The distribution function F [Eq. (4.1)] of the reduced diffusion rate D^* [Eq. (4.5)] in model (2.2) without invariant curves ($d = 0$). The thick dashed straight line represents asymptotic behavior (4.6) of the integrated D distribution (4.2) for the Gaussian p statistics. Two lower wiggly lines correspond to large deviations from the Gaussian statistics: $D_* = 42$ ($K = 10^{-3}$) and 461 ($K = 3 \times 10^{-5}$) (see insert). A group of ten D distributions in a large interval ($10 \leq D_* \leq 461$) are brought together using empirical relation (4.9). Insert: the shift factor R_D vs. the deviation D_* [Eq. (4.8)] for $K = 10^{-3}$ (circles) and 3×10^{-5} (crosses); the straight line is empirical relation (4.7).

which are the mean and the variance, respectively. For the Gaussian p distribution, the reduced variance in Eq. (3.2) becomes $V_M = 1$, and therefore,

$$\left(\frac{\Delta D}{\langle D \rangle}\right)^2 = \frac{1}{\lambda} = 2 \qquad (4.4)$$

and $\lambda = 1/2$ is independent of α. Moreover, if we introduce the dimensionless diffusion rate

$$D \longrightarrow D^* = \frac{D}{D_\infty} \qquad (4.5)$$

with the average $\langle D^* \rangle = 1$, we also obtain from Eq. (4.3) that $\alpha = \lambda = 1/2$. The new distribution then becomes

$$f(D^*) = \frac{(D^*)^{-1/2} \exp(-D^*/2)}{\sqrt{2\pi}}$$

and

$$F(D^*) = \int_0^{D^*} f(D')dD' \longrightarrow \sqrt{\frac{2}{\pi}D^*}, \qquad (4.6)$$

where the latter expression gives the asymptotic behavior as $D^* \longrightarrow 0$ that we need. This asymptotic form is

in very good agreement with the empirical data in Fig. 2 even at $D^* \approx 0.1$ (!). For very small D^*, the accuracy of the agreement is limited by the fluctuations caused by several remaining points. The smallest value $D^* = 8.3 \times 10^{-11}$ corresponds to the estimate $D^*_{\min} \sim 1/J^2 = 10^{-10}$.

Because the distribution $f(D^*)$ in (4.6) is also Gaussian in $\sqrt{D^*}$, the integral $F(D^*)$ admits a very simple approximation found in [18],

$$F(D^*) = \begin{cases} 1 - \dfrac{\exp(-D^*/2)}{\sqrt{D^* + 1}}, & D^* > 1/2 \\[2mm] \sqrt{\dfrac{2D^*}{\pi}}, & D^* < 1/2. \end{cases} \qquad (4.6a)$$

The relative accuracy $|\Delta F/F| < 0.05$ of this approximation is better than 5% in the entire range of F. Actually, the accuracy is even much better except in a narrow interval at $D^* \sim 1/2$.

Thus, the upper distribution in Fig. 2, which describes the real diffusion at a sufficiently long motion

time, is in a good agreement with the available theory. This is no longer the case for the lower distribution on the plateau. In itself, this is not a surprise, because, contrary to the previous case, the measured diffusion rate is mainly determined by nondiffusive processes. But a very interesting feature of this nondiffusive distribution is that the exponent of the power-law tail remains exactly the same as if the p distribution were a Gaussian one. The simplest explanation, quite plausible to us, is that the far tail still represents a distribution that is a part of the entire distribution according to our original picture expressed by estimate (3.1). One immediate inference is then the decrease in the tail probability if we use the same variable $D^* = D/D_\infty$. This is indeed the case according to the data in Fig. 2!

A more difficult problem is the quantitative estimate of the distribution shift for the motion time $t \lesssim 1/K$ with the ratio $\langle D^* \rangle = \langle D(t) \rangle / D_\infty > 1$. This shift can be characterized either via the probability decrease by R_F times for a fixed D^* or via the increase in D^* itself by R_D times for a fixed probability. We note that $R_D = R_F^2$ on the tail because of the square-root dependence in Eq. (4.6). The characteristic R_D seems more preferable to us because it describes the shift not only of the tail but also (qualitatively) of the entire distribution $F(D^*)$.

Having analyzed the data, we found the empirical relation for the tail shift,

$$R_D(D_*) \approx D_*^a, \tag{4.7}$$

where the new diffusion ratio is

$$D_*(\tau) \approx \frac{D_0}{\tau D_\infty} + 1 \tag{4.8}$$

and the fitted exponent is $a = 0.45$.

The philosophy behind this relation is as follows. We start with our original picture of a combined diffusive/nondiffusive process described by Eq. (3.1), which is almost our final choice (4.8). But at the beginning, we seemed to improve the original relation by including our surprising discovery, the plateau. Specifically, we tried to use Eq. (3.5), which is in good agreement with the empirical data, for the dependence $D(t)$ (see Fig. 1). We also found that it partly describes the distribution $F(D)$, except on that mysterious plateau! Our final step was then to return from (3.5) to a version of (3.1) in form (4.8).

Although it may have seemed strange, this did work with a reasonable accuracy, as the inset in Fig. 2 demonstrates. The question "why?" is still to be answered in further studies. This is actually a serious general problem of the dynamical mechanism underlying the plateau formation and statistics.

Our empirical relation (4.7) can be represented differently. Namely, instead of describing the actual distribution tail shifted with respect to the asymptotic form in Eq. (4.6), we can introduce the scaled diffusion rate

$$D \longrightarrow \frac{D}{R_D},$$

which implies that

$$D^* \longrightarrow \frac{D^*}{R_D}. \tag{4.9}$$

The result is shown in Fig. 2 as a beam of ten scaled distributions scattered around asymptotic line (4.6).

5. DIFFUSION AMID VIRTUAL INVARIANT CURVES: THE LYAPUNOV EXPONENTS

In the previous sections, we considered a very particular and simplest limiting case of our model (2.2) with the parameter $d = 0$. In this case, the motion is ergodic [6], which greatly simplifies the problem under consideration. Nevertheless, we obtained a number of new results that form a firm foundation for further studies.

The most important new feature of the motion for $d > 0$ is the so-called divided phase space of the system, that is, a mixture of both chaotic and regular components of the motion. This is a typical structure of dynamical systems with several degrees of freedom (see, e.g., [4]).

First of all, we must eliminate the regular trajectories from further analysis of the diffusion statistics. The standard well-known method to achieve this consists in simultaneously computing for each trajectory the so-called Lyapunov exponent Λ, which is the rate of the local exponential instability of the motion (see, e.g., [1–3] and references therein). A two-dimensional canonical (Hamiltonian) map such as our model (2.2) involves two Lyapunov exponents whose sum is always zero, $\Lambda_1 + \Lambda_2 = 0$. For a chaotic trajectory, one exponent, e.g., $\Lambda_1 = \Lambda_+ > 0$, is positive and the other is negative, $\Lambda_2 = \Lambda_- < 0$. As a result, in accordance with the standard definition of the Lyapunov exponent in the limit as $t \longrightarrow \infty$, any tangent vector (dx, dp) of the linearized motion approaches the eigenvector corresponding to $\Lambda_+ > 0$.

A simple well-known procedure for computing Λ_+ that we also use in the present work is as follows. For each of M trajectories with random initial conditions x_0 and p_0, we chose the tangent vector (dx, dp) of a random direction and the unit modulus, $d\rho^2 = dx^2 + dp^2 = 1$. Both maps, the main one and the one linearized with respect to the main reference trajectory $x(t, x_0, p_0)$, $p(t, x_0, p_0)$, were then run simultaneously during some time t. The current $\Lambda(t)$ was finally calculated from the standard relation

$$\Lambda(t) = \frac{\langle \ln \rho(t) \rangle}{t}, \tag{5.1}$$

where the brackets denote averaging over M trajectories. In contrast to the formal mathematical definition of Λ in the limit as $t \longrightarrow \infty$, the Lyapunov exponent $\Lambda(t)$ is always time-dependent, perforce, in numerical experiments.

In Fig. 3, several typical examples of the Λ distribution are depicted for the number of events in (4.1) $J = M$ equal to that of trajectories and with a smaller number of printed points $J_0 = M' \le M$ except in the case where $d = 0$. The simplest distribution is for the ergodic motion ($d = 0$). It has the form of an almost vertical step, whose derivative $dF/d\Lambda \sim 10^4$ is a very narrow δ function. We note that the regular chain of points along the F axis has no special physical meaning but simply reflects a particular type of distribution accepted, $F(\Lambda_j) = j/J$ with integer j [see (4.1)]. The mean value of Λ depends only on K [see Eq. (2.10)] but not on the initial conditions. This example in Fig. 3 shows the empirical/theoretical ratio, which is very close to unity, as expected.

The other two examples correspond to the same values $K = 0.45$ and $M = 10^4$ but different motion times $t = 10^4$ and 10^5 iterations. Both distributions have the same step at the largest Λ, which corresponds to diffusive components (not necessarily a single one) of the motion, similarly to the ergodic case. But the most interesting part is the rest of the distribution, which represents a rich motion structure, contrary to a dull one in the ergodic motion.

The largest (but not the most interesting) part of this structure is related to the steep distribution cutoff at small Λ. Comparison of the two distributions for different motion times $t = 10^4$ and 10^5 shows that, in this region, the Λ values of the trajectories decrease with increasing time approximately as $\Lambda \sim 1/t$. This means that all these trajectories are regular [see Eq. (5.1)] because the tangent vector ρ does not grow. The relative number of such trajectories gives the total area of regular motion on the phase cylinder of the system. In the example under consideration, it is given by $A_{\mathrm{reg}} = 3177/10\,000 \approx 0.318$ ($t = 10^5$). Generally, this value depends on a particular choice of the cutoff border (see the arrow in Fig. 3). This delicate experimental problem is considerably mitigated by a fortunate feature of the Λ distribution in our model, namely, the occurrence of a relatively wide plateau of $F(\Lambda)$ immediately above the cutoff with only several trajectories on it. But the statistical accuracy

$$\frac{\Delta A_{\mathrm{reg}}}{A_{\mathrm{reg}}} \approx (MA_{\mathrm{reg}})^{-1/2} \qquad (5.2)$$

is typically much worse and can be improved by increasing the number of trajectories (and the computation time) only.

Another interesting feature of the Λ distribution in our model is a characteristic "fork" shape of the cutoff. This is a result of negative Λ for many regular trajecto-
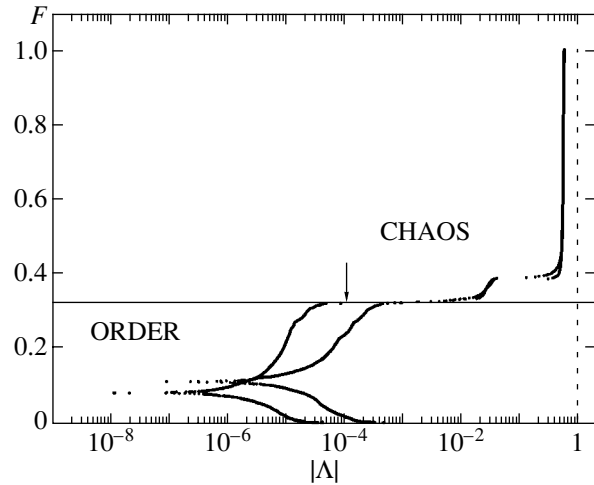

Fig. 3. Examples of the distribution function $F(\Lambda)$ of type (4.1) with the Lyapunov exponent in model (2.2) for $d = 0$, $M = M' = 80$, $t = 10^4$ (the rightmost step $F(\Lambda)$, ergodic motion) and for $d = 1/2$, $M = 10^4$, $M' = 1000$, $t = 10^4$, 10^5 (nonergodic motion); in all cases, $K = 0.45$. The horizontal line indicates the total share $A_{\mathrm{reg}} \approx 0.318$ of the motion regular components. The arrow at $\Lambda = 10^{-4}$ shows the lower border of chaotic trajectories chosen for further analysis (for $t = 10^5$).

ries. Such a peculiar representation is obtained by ordering $\Lambda(t)$ values with their signs but plotting the moduli $|\Lambda(t)|$ only. The lower prong of the fork therefore corresponds to $\Lambda(t) < 0$, while $\Lambda(t) > 0$ on the upper one. This is because of the complex-conjugate Lyapunov exponents, resulting in a strictly bounded oscillation of the tangent vector (dx, dp) in this case. However, the area $A_\pm$ [see Eq. (5.4) in what follows] is noticeably smaller than the total area of regular domains A_{reg}, $A_\pm \approx 0.20 < A_{\mathrm{reg}} \approx 0.318$. The rest is filled with trajectories that are also regular but linearly unstable.

This implies the linear growth of the tangent vector in time, $\rho(t) \sim t$, such that $\Lambda(t) \longrightarrow 0$ remains positive but vanishes in the limit as $t \longrightarrow \infty$. This is the so-called marginal local instability with both $\Lambda_\pm = 0$ equal zero (see [19] for a discussion). A curious point is that this seemingly exceptional case becomes the typical one in a nonlinear oscillator system because oscillation frequencies depend on the trajectory initial conditions. In fact, the bounded ρ oscillation producing negative $\Lambda(t)$ is the exceptional case. The origin of this peculiarity is in a piecewise linear force in our model (2.2). As a result, the motion in the main (and, for large K, the biggest) regular domain around the fixed point $x = 1/2$, $p = 0$ is precisely the harmonic oscillation with the frequency (for $K < d$)

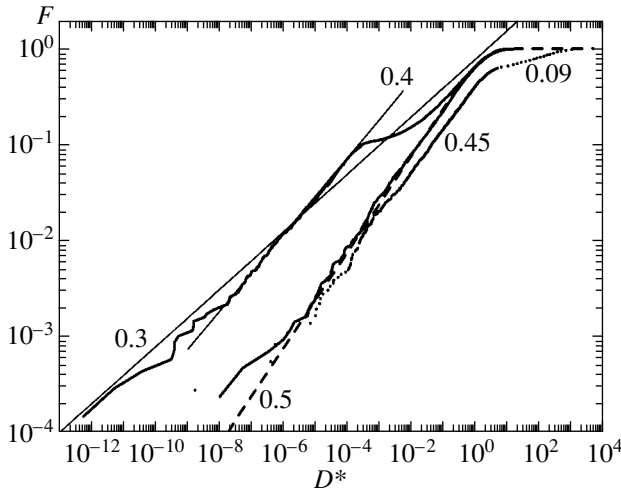$$\Omega = \arccos\left(1 - \frac{K}{d}\right) \approx 1.47, \qquad (5.3)$$

Fig. 4. Three characteristic examples of the diffusion statistics in the critical structure including virtual invariant curves ($d = 1/2$). Shown are the integral distributions F [Eq. (4.1)] of the normalized diffusion rate $D^* = D/D_{norm}$. The numbers at the curves are the critical diffusion exponents c_m. The largest one $c_0 = 0.5$ corresponds to the ergodic motion ($d = 0$) without any critical structure (the dashed curve). Two straight lines show the averaged ($c_1 = 0.3$) and local ($c_1' = 0.4$) critical exponents for $K = 0.45$ (the solid line connecting 500 values of $F(D^*)$). The distribution for $K = 0.335$ with two local critical exponents ($c_2 = 0.09$ and $c_2' = 0.45$) is represented by 300 points shifted to the right to avoid overlapping with the other two distributions. The third distribution (a solid line through 1000 points, $K = 0.3294$) is surprisingly close to that in the ergodic case (dashed line). In all three examples, $M = 10^4$, $t = 10^5$.

which remains the same in the entire regular domain of the area

$$A_{\pm} = \frac{2\pi K}{d} y_{\pm}^2 \left(1 - \frac{K}{2d}\right) \approx 0.20. \qquad (5.4)$$

Here, $y_{\pm} = x_{\pm} - 0.5 = \pm d/2$ is the position of two singularities of the force (see Eq. (2.2) and below) that restrict the size of the regular domain surrounded by the limiting ellipse to which both lines of the singularity $y_{\pm} = d/2 = 0.25$ are tangent. This ellipse is determined by the initial conditions

$$p_0 = 0, \quad x_0 = 0.5 + y_{\pm}\left(1 - \frac{K}{2d}\right) \approx 0.5 \pm 0.185. \quad (5.5)$$

All the numerical values above correspond to $K = 0.45$ and $d = 1/2$. Within the ellipse, the motion of the tangent vector obeys the same equation as the main motion, the only difference being an arbitrary length ρ of the tangent vector (for details, see [3] and references therein).

Returning to Fig. 3, we note that the measured area $A_{\pm}$ decreases as the motion time increases. This is explained by the penetration of trajectories into a very

complicated critical structure at the chaos border surrounding each regular domain (for details, see, e.g., [4]). For the same reason, the direct measurement of the entire regular region $A_{reg} \approx 0.40$ by a single chaotic trajectory for 10^9 iterations gives a noticeably larger value compared to $A_{reg} \approx 0.318$ obtained from 10^4 trajectories with 10^5 iterations each.

With all the curiosity of the $\Lambda(t)$ distribution being in regular components of the motion, our main interest in the present study is in the intermediate region between the regular cutoff at smallest $\Lambda(t) \longrightarrow 0$ and the chaotic step at maximum Λ independent of t. In this region, the distribution is also independent of the motion time and characterizes the proper critical structure of the chaotic motion. In the example in Fig. 3, this structure is represented by a relatively small probability step $\Delta F \approx 0.06$ at $\Lambda \approx 0.03$. Several other examples are also considered in the next section.

6. DIFFUSION AMID VIRTUAL INVARIANT CURVES: THE CRITICAL STATISTICS

In Fig. 4, we present three characteristic examples of the effect of the critical structure on the diffusion statistics. The dashed curve shows the "unperturbed" distribution $F(D^*)$ of the normalized diffusion rate $D^* = D/D_{norm}$ [see Eq. (4.1)], with the normalizing rate D_{norm} to be chosen in each particular case (see below). The term "unperturbed" refers to the ergodic case $d = 0$ without any invariant curves and critical structure (see Section 4; the problem of the critical structure in this case is not as simple as it may seem; see below and Section 7). The normalizing rate $D_{norm} = D_{\infty}$ is then the true asymptotic diffusion rate (4.5).

We are now interested in the effect of the critical structure that typically arises in a nonergodic motion with its barriers for the chaos, or chaos borders. The latter are a particular, and a very important, case of an invariant curve transformed into itself under the dynamics of the system. As discussed in Section 1, there are several different types of invariant curves.

One is the well-studied and rather familiar chaos border surrounding any domain with regular motion. In this paper, we call it the local invariant curve (LIC); it does not block the global diffusion around such a domain. An important property of a LIC is the robustness, which means that a small change of the system, e.g., of the parameter K or d, cannot destroy the LIC but can only deform it slightly. This implies that LICs are always present in any divided phase space.

Here, we are mainly interested in invariant curves of a different type, the global invariant curves. Each GIG cuts the entire phase-space cylinder (x mod 1) of our model and therefore completely prevents global diffusion in p. Such invariant curves are less known, especially the most surprising of them, the separatrix of a nonlinear resonance. But those GICs are not robust in the model under consideration (see [9]), being

destroyed by almost any arbitrarily small perturbation of the system, in particular by a change of even a single one of its parameters. In other words, such GICs exist only for special values, e.g., $K = K_m$. Although there are typically infinitely many such special values, the probability of finding a GIG in a randomly chosen system is zero. This is why we are interested in a more generic situation where our model has no GICs at all. But the effect of those still persists in a certain domain around each K_m! For this reason, we call such GICs virtual invariant curves (VICs) in analogy with other virtual quantities in physics, e.g., virtual energy levels in quantum mechanics. We note that unlike a GIG, a VIC is robust and, hence, generic.

Both LICs and GICs produce the so-called critical structure of motion (see, e.g., [4]), which is typically characterized by a power-law distribution of principal quantities. The corresponding exponents c_n are called critical exponents. Their values are shown in Fig. 4 at the related distributions. We note that the opposite is generally not true; that is, a particular power law does not necessarily indicate any critical structure. In our model, this is the case for the ergodic motion where the diffusion rate distribution is also characterized by an asymptotic ($D \longrightarrow 0$) power law with the exponent $c_0 = 0.5$ (see above and Section 7). An important difference between ergodic and nonergodic dynamics, however, is that, in the latter case, all the critical exponents $c_n < c_0$ are less than the (generally noncritical) ergodic exponent c_0. This is the main physical result of our preliminary numerical experiments that we can present and already discuss now (see Fig. 4).

We start with the distribution for $K = 0.45$ (the upper solid line), which is far in the region without VICs (the border of this region is at $K_B(d = 1/2) = 1/3$; see Eq. (2.3) above and [16]). But the regular trajectories ($A_{\text{reg}} \approx 0.318$) together with LICs and the related critical structure are present. As a result, the distribution (with $D_{\text{norm}} = D_\infty$) deviates considerably from the unperturbed one for the ergodic motion with $d = 0$. The critical structure of this type in a relatively narrow layer around a LIC is well studied by now (see, e.g., [4]), including the case where the typical distribution deviates from a pure power law. The latter would imply the exact scale invariance of the underlying critical structure in both the system phase space and its motion time.

The critical structure is described by the so-called renormalization group, or renormgroup for brevity. On the other hand, the equations of motion also form a certain (dynamical) group for any dynamical system. Such a fundamental similarity allows interpreting the critical structure as a certain dynamics, which was called the renormdynamics [4, 20]. In this picture, the exact scale invariance with a pure power-law distribution corresponds to the simplest, periodic renormdynamics, even though the original dynamics may be the most complicated chaotic motion. The resolution of this apparent paradox is that the complexity of the original dynamics is "transferred" to the dynamical infinite-dimensional space of the renormdynamics, leaving behind the simplest renormdynamics itself (sometimes!).

This case is best studied only because it is the simplest one. But the generic case is just the opposite—a typical renormchaos is also chaotic [20, 21]. This implies a certain chaotic oscillation of the characteristic distribution around some average power law. This is precisely the case for the upper distribution in Fig. 4. It is characterized by the average critical exponent $c_1 = 0.3$ with fluctuations of the order $c_1' - c_1 = 0.1$. Such an interpretation of the critical structure in question is known to be typical but not necessarily unique (see below). The truly unique property of this critical structure is the infinite power law, with or without fluctuations. The term "infinite" here corresponds to the range of a renormdynamical variable $\ln D \longrightarrow -\infty$ with an unrestricted variation, even though the diffusion rate itself $D > 0$ is strictly bounded from below.

This is no longer the case for the critical structure of a new type that we have encountered in our problem and which is produced by VICs (=robust GICs) rather than by robust LICs. As explained above, the principal difference between the two is that the VIC is not an invariant curve at all. In terms of renormdynamics, this implies that a VIC can mimic a GIC for relatively large $\ln D$ only. This is clearly seen in Fig. 4 in the upper part of the distribution with the local critical exponent $c_2 = 0.09$ and the parameter $K = 0.335$ (points). Here, we have taken $D_{\text{norm}} = 10^{-6} < D_\infty \approx 2 \times 10^{-5}$ much smaller than the true diffusion rate D_∞. This shifts the entire distribution to the right in order to avoid overlapping with other distributions. This value is slightly above the border $K_B(1/2) = 1/3$ [see Eq. (2.3)], where there are many VICs without any GIC. As a result, the range of the characteristic critical exponent c_2, $\Delta \ln D^* \approx 5$ is very short compared to the total available range ≈ 25. The rest of the distribution remains sufficiently close to the unperturbed one. This implies the absence of the critical structure or its sharp change at $\ln D \lesssim 2$ at least. With this interpretation, the renorm-motion stops in the specified region.

This in turn implies a "dissipative" rather than "Hamiltonian" renormdynamics. We note that the main part of the distribution is close but not identical to the unperturbed one because of a slight difference in the characteristic exponent. Whether this implies a certain very slow renorm-motion remains a very interesting open question. Interestingly, the larger critical exponent $c_2' = 0.45$ is also close to the local critical exponent $c_1' = 0.4$ in the region without VICs or GICs; above, it was interpreted as a random fluctuation in renormchaos. Whether this is indeed true remains unclear.

Finally, the third distribution in Fig. 4 (the lower solid line) actually coincides with the unperturbed distribution ($D_{\text{norm}} \approx D_\infty$), even though it corresponds to the

region with many VICs and a strong suppression of the diffusion ($K = 0.3294$—see Fig. 3 in [16]). A deviation for very small D^* is due to poor statistics at this end. We note that the coincidence of both distributions is not only asymptotic (as $F \longrightarrow 0$), but also complete, including the opposite limit as $F \longrightarrow 1$. This occurs in spite of a rather large regular region $A_{reg} \approx 0.581$. The origin of this peculiarity for a particular K value remains unclear. One possibility is that the area of the critical structure at the chaos border around this regular domain is unusually small for some reason. Examples of such a peculiarity are known in different models (see [22]) where the critical structure was found to be unusually large but hidden. In other words, the motion was ergodic but with strong correlations [cf. the unusual diffusion rate in Eq. (2.8) for $K \ll 1$ in the ergodic system at $d = 0$]. Returning to this case in Fig. 4, we conclude that our "unperturbed" power-law distribution with the exponent $c_0 = 0.5$ (dashed line) may well represent a peculiar critical structure related to the strong hidden temporal correlations rather than to a purely spatial geometry of the phase space. If this is true, the correlation decay may indeed be not a power-law one, as is the case in the model in [22], where such a hidden decay is purely exponential (see Fig. 6 in [22]).

We finally mention another peculiarity of the critical structure in question: all the critical exponents found so far are smaller, albeit by a small amount, than the "unperturbed" or "hidden" one $c_0 = 0.5$. The physical meaning of this universal inequality is that the critical structure under consideration always increases the probability of a very low diffusion rate $D \longrightarrow 0$. The general mechanism of this effect is known (see, e.g., [4]) and is explained by the trajectory "sticking" within a complicated critical structure, which slows down the diffusion. Interestingly, the sign of the sticking effect can be opposite when the sticking accelerates the diffusion up to the absolute maximum $D(t) \propto t$ of the homogeneous diffusion rate [23, 24].

To summarize, we see that our "simple" model considered in this paper reveals a great variety of critical structures still to be further studied and understood.

7. CONCLUSION:
A HIDDEN CRITICAL STRUCTURE?

In this paper, we present some preliminary results of the numerical experiments with a family of simple models specified by the smooth canonical 2D map (2.1) with global virtual invariant curves. As in [16], we use here the same strongly chaotic model and again focus on the statistics of the diffusion rate D, which proves to be of a very complicated (apparently fractal) type determined by the so-called critical structure of both the phase space and the motion (see, e.g., [4]). In [16], we studied the statistics of the mean diffusion rate $\langle D(K) \rangle$ averaged over the ensemble of trajectories with random initial conditions. Our main result there was the observation of very big and irregular fluctuations of the dependence $\langle D(K) \rangle$ and a long and very slowly decaying tail of the $\langle D \rangle$ distribution as $\langle D \rangle \longrightarrow 0$. We termed the latter effect the VIC diffusion suppression.

In the present paper, we continue studying this interesting phenomenon in more detail. For this, we pass from the statistics of averages $\langle D(K) \rangle$ as functions of the model parameter K to the statistics of individual trajectories for a given K. In principle, this approach provides the deepest insight into the statistical problem. As the main statistical characteristic, we have chosen the integral distribution $F(D)$ in form (4.1) for poor statistics as $\langle D \rangle \longrightarrow 0$. Preliminary results of our extensive numerical experiments presented in Fig. 4 confirm our earlier conjecture on a critical structure underlying the fractal dependence $\langle D(K) \rangle$ in [16], the true sign of such a structure being various power-law distributions found. Moreover, in addition to the familiar well-known critical structure exemplified in Fig. 4 by the case with the parameter $K = 0.45$, we observed many cases of a rather different structure, as the one with $K = 0.335$. The principal difference of the latter is its finite size in the structure variable $\Delta \ln D \lesssim 5$. A natural explanation of this difference is as follows. First, the VIC is not a true invariant curve like a GIC. The latter completely blocks the global diffusion, while the former can at most inhibit the diffusion only. The mechanism of inhibition is known to be the trajectory sticking inside a very complicated critical structure. The sticking is the stronger (longer), the smaller the spatial and/or the longer the temporal scale of the critical structure. But for the VIC structure, both scales are strictly limited. On the other hand, this restriction is the weaker, the higher the VIC density. In the system under consideration, the VIC density is rather large, and hence, the restriction leaves enough freedom for a strong suppression of the global diffusion for almost any K. Moreover, because the critical exponent of the VIC structure is typically very small (for example, $c_2 = 0.09$ in Fig. 4), the probability of large suppression is high even for a short critical structure (cf. [16] for a different characteristic of this phenomenon). This slowly decaying suppression probability is well ascertained in our numerical experiments, but we have no theoretical explanation of such behavior.

We now come to possibly the most interesting result of our current studies. Strange although it may seem, this brings us to the apparently simplest case of our model with $d = 0$, when the motion is ergodic. The problem is whether it can still reveal any structure on the grounds that the distribution $F(D)$ is also a power law (Fig. 4). This is certainly not the case if in addition $K \gg 1$ and the diffusion rate has standard form (2.11), $D \propto K^2$. But if $K \ll 1$, the diffusion rate becomes qualitatively different at least, $D \propto K^{5/2}$. This does not imply anything in general. But in the particular case under consideration, this dependence $D(K)$ can be, and actually was, derived [16] from the resonance structure of

motion. If the system were not ergodic (with a divided phase space), this structure would be clearly seen in the phase space. The question is what happens for the ergodic motion with the same dependence $D(K)$. In [16], we conjectured that some structure would persist in the form of correlations that determine the diffusion rate, which is in some "hidden" form and cannot be directly seen in the picture of the motion in phase space. An example of such a hidden critical structure was found in [22] (see Section 6). But in that case, a particular distribution function was exponential rather than a power-law one(?). Hence, the question is whether this qualitative difference can depend on a particular characteristic of the critical structure. Another question arises from a very strange temporal behavior of the diffusion rate in the same "simple" case of the ergodic motion for $d = 0$—a "mysterious" plateau at the very beginning of diffusion under a weak perturbation ($K \ll 1$; see Fig. 1). In this case, the dependence $D(K) = K^2/3$ is the same as in the opposite limit of strong ($K \gg 1$) uncorrelated perturbation(?) but for a very short time only, the shorter the stronger the perturbation(?!). Moreover, the correlations on the plateau not only are very large as in the weak-perturbation limit $K \longrightarrow 0$ but also increase during the entire plateau regime [see Fig. 1, dashed lines for the variances $V_M(\tau)$ in Eq. (3.2)]. At present, we have no definite explanation for this controversial behavior. A discreet current conjecture is as follows. The duration of the plateau is $t_{pl} \approx 1$, or $\tau_{pl} \approx 1/\Lambda \approx 1/\Omega$ [see Eq. (2.9)]. But the latter expression gives the phase oscillation period on the critical nonlinear resonance that determines the diffusion rate [16]. One can then imagine that this period characterizes not only the correlation decay, as usual, but also the correlation uprise. But, the invariable diffusion rate over the entire plateau region is yet to be explained.

ACKNOWLEDGMENTS

REFERENCES

1. B. V. Chirikov, Phys. Rep. **52**, 263 (1979).
2. G. M. Zaslavsky and R. Z. Sagdeev, *Introduction to Nonlinear Physics* (Nauka, Moscow, 1988).
3. A. J. Lichtenberg and M. A. Lieberman, *Regular and Chaotic Dynamics* (Springer-Verlag, New York).
4. B. V. Chirikov, Chaos, Solitons, and Fractals **1**, 79 (1991).
5. J. Moser, *Stable and Random Motion in Dynamical Systems* (Princeton Univ. Press, Princeton, 1973).
6. I. Dana, N. Murray, and I. Percival, Phys. Rev. Lett. **62**, 233 (1989).
7. B. V. Chirikov, E. Keil, and A. Sessler, J. Stat. Phys. **3**, 307 (1971).
8. M. Hénon and J. Wisdom, Physica D (Amsterdam) **8**, 157 (1983).
9. S. Bullett, Commun. Math. Phys. **107**, 241 (1986).
10. M. Wojtkowski, Commun. Math. Phys. **80**, 453 (1981); Ergodic Theory Dyn. Syst. **2**, 525 (1982).
11. L. V. Ovsyannikov, private communication (1999).
12. V. V. Vecheslavov, nlin.CD/0005048.
13. V. V. Vecheslavov, Zh. Éksp. Teor. Fiz. **119**, 853 (2001) [JETP **92**, 744 (2001)].
14. V. V. Vecheslavov, Preprint No. 99-69 (Budker Institute of Nuclear Physics, Novosibirsk, 1999).
15. V. V. Vecheslavov and B. V. Chirikov, Zh. Éksp. Teor. Fiz. **120**, 740 (2001) [JETP **93**, 649 (2001)].
16. V. V. Vecheslavov and B. V. Chirikov, Zh. Éksp. Teor. Fiz. **122**, 175 (2002) [JETP **95**, 154 (2002)].
17. D. Sornette, L. Knopoff, Y. Kagan, and C. Vanneste, J. Geophys. Res. **101**, 13 883 (1996).
18. B. V. Chirikov and O. V. Zhirov, nlin.CD/0102028.
19. G. Casati, B. V. Chirikov, and J. Ford, Phys. Lett. A **77**, 91 (1980).
20. B. V. Chirikov and D. L. Shepelyansky, Physica D (Amsterdam) **13**, 395 (1984).
21. S. Ostlund, D. Rand, J. Sethna, *et al.*, Physica D (Amsterdam) **8**, 303 (1983).
22. B. V. Chirikov, Preprint 1999-7 (Budker Institute of Nuclear Physics, Novosibirsk, 1999).
23. B. V. Chirikov and D. L. Shepelyansky, Phys. Rev. Lett. **82**, 528 (1999).
24. B. V. Chirikov, Zh. Éksp. Teor. Fiz. **119**, 205 (2001) [JETP **92**, 179 (2001)].